EUROPEAN JOURNAL OF MATERIALS SCIENCE AND ENGINEERING
Volume 7, Issue 1, 2022: 049-071 | www.ejmse.ro | ISSN: 2537-4338

EJMSE

DOI: 10.36868/ejmse.2022.07.01.049

SACCHARUM MUNJA DERIVED BIOCHAR LOADED WITH HEMATITE NANOMATERIAL FOR REMEDIATION OF CHROMIUM(III) FROM AQUEOUS ENVIRONMENT: ISOTHERMAL, ERROR ANALYSIS, KINETIC AND THERMODYNAMIC STUDIES

Tunzeel IQBAL[1,*], Shahid IQBAL[2], Fozia BATOOL[1]

[1]Department of Chemistry, University of Sargodha, Sargodha, Sargodha 40100, Pakistan.
[2]University of Education, Jauharabad Campus, University of Education Jauharabad 41200, Pakistan.

Abstract

Three forms of Saccharum munja had been utilized for a comparison among uptake of chromium metal from aqueous media. Scanning electron microscope characterization of sorbents revealed microporous and tubular structure in modified nanomaterial. Fourier transform infrared analysis explored different surface attaching ionic groups like hydroxyl, carbonyl also nitro groups, responsible for metal uptake from solution. Experiments on concentration factor suggested maximum percent sorption capacity of 89.65 by hematite loaded Saccharum munja biochar. Adsorption equilibrium data implication on isotherms and error functions favored experimental findings. Calculation of two forms of different isotherms for example Dubinin-Radushkevich, Langmuir, Temkin and Freundlich isotherm supported adsorption experiments with high R^2>0.9 values for all sorbents. Error analysis indicated favorable results by five errors but chi-square test error values were minimum in both linear data and non-linear data. Kinetic modeling results indicated high rate of adsorption as shown by their large R^2 value and closely related k, Qe and h values. Thermodynamic results showed that biosorption reactions were endothermic and spontaneous. These results also suggest that hematite loaded nanomaterials are good biosorbents for chromium metal uptake in minimum concentration and high output. Desorption study was essential for recovery of nanomaterial to be used again and again in experiments.

Keywords*: Adsorption, biochar, equilibrium, nanomaterial, Saccharum munja*

Introduction

Thermal decomposition of organic material at low temperature produces biochar [1]. Since biochar material is generated as result of pyrolysis of a diverse range of biomass organic matter and refers to high carbon solid [2]. During thermal conversion, volatile organic mass is lost and volume reduction occurs, but original carbonaceous material retains its structure and porosity [3]. Porosity and surface area are indicators about molecular structure of biochar [4]. X-ray diffraction determines amorphous nature of biochar and presence of aromatic compounds, as highly conjugated crystalline structures [5]. These crystalline areas are referred as conducting phase flattened sheets, which are aromatic and cross-linked randomly [6].

Biomass feedstock is converted into biochar to enhance surface structural properties. Biomass properties including cellulose, hemicellulose, lignins, pre-handling conditions and inorganic composition also affect all the above properties. Additionally, conditions of biochar production process, contribute to the properties of final product, such as reaction time, temperature, and reactor type. Industrial activation processes can increase porosity and surface

*Corresponding author: tunzeel16@gmail.com , fozia.batool@uos.edu.pk

area of biochar which include physical and chemical activation. Biochar micropores (50 nm diameter) generally facilitate a variety of filtration applications including both aqueous and gaseous filtration by adsorption of small molecules. On the other hand, macropores are responsible for water absorptivity, soil aeration, large particle binding, microbial habitat facilitation, and bulk volume

Mixing of biochar with soil has been reported to improve fertility, structural modification and physicochemical properties of soil such as water holding capacity, ion exchange capacity and aeration conditions [7]. It is mainly used for soil management to improve soil nutrient contents, carbon sequestration and pollutants control [8]. Biochar has its established applications as soil conditioner several thousand years ago, but now it has been used widely in other fields. Biochar production helps to achieve recovery of energy and waste minimization. Pyrolysis helps to reduce weight and volume of the waste biomass feedstock, hence, minimizes its waste disposal space. Biochar as an adsorbent have potential to remove organic and inorganic pollutants from different sources. Its huge number of oxygen saturated functional groups facilitate adsorption of compatible species [8].

In addition to traditional materials, nanosized adsorbents owing to preferable large surface capacity, indicate an increase in percentage efficiency and high adsorption rate. In this way, various novel nanostructures have been developed to treat all sort of polluted water. To remove metals and dyes nanocomposites have been considered as low cost and environment safe materials [9]. Nanomaterials have gained importance in current years in preparation and fabrication of new composite structures [10]. Nanoscience advancement and assembly of new nanomaterials have broadened ways of pollution control especially non-biodegradable metals [11]. To fabricate nanomaterials, a large no. of methods have been developed, but the focus is to create those materials which are low cost and energy saving in reactions [12]. High surface adsorption capacity is provided by biochar to adsorbate species. Also, the nanomaterial synthesis and application on biochar enhances adsorption owing to presence of more activated groups on adsorbent sites.

Toxic metals are now labeled as high priority pollutants pertaining to their mobilization and accumulation in environment. There is a significant increase in industrial use of these metals causing water bodies pollution [13]. these metals have deleterious effect on both plants and animals, after they enter into water streams and uptaken by both of them [14]. Toxicity caused by these metals is dependent upon their In industries using chromium compounds, there is dire risk in inhalation of chromium bearing aerosols in respiratory track. Absorption through inhalation in lungs depends upon characteristics of aerosols such as, size, shape and hygroscopicity. Cr(VI) compounds such as chromate are carcinogenic and cause respiratory diseases e.g. lungs cancer owing to large contact with chromate salt of sodium [15]. Tanneries and textile industrial effluents mostly consist of lead, cadmium, iron, chromium, zinc and nickel which act as human carcinogens and also accumulate in agricultural soil to affect quality production of crops [16]. Concentration of chromium in water bodies including sea water, surface water and rain water has been calculated to be 0.00004-0.0005 ppm, 0.001 to 0.010 ppm and 0.0002 to 0.001 ppm. Chromium concentration in soil has been reported to be 10-100 mg/Kg. oxides and hydroxides of chromium also occurs in the air from manmade sources.

Climate variations are contributing towards decrease in useable water level and for sustainable availability of clean water its purification is necessary from easily available sources [17]. During past few years, bio waste materials are used for the removal of contaminants from aqueous media and industrial effluents. These biomaterials include plant or animal wastes, microorganisms or their modified forms. Owing to their availability, low cost and efficiency in metal removal due to presence of certain functional groups such as amino or hydroxyl groups, these materials are now widely used as biosorbents [18]. Selective adsorption by nano-particles, fertilizer industrial waste, red mud, coal, biomass and algae has created great attention in this field [19, 20]. Different byproducts obtained from industries such as wasted iron, slags of iron,

fly ash and hydrous titanium oxide are chemically modified to enhance their efficiency to remove metals from polluted water. Recently, heavy metals have been removed by agricultural feedstock by biosorption process. Adsorption process describes a group of procedures, which includes adsorption and precipitation reactions involving the transfer of ions from solution phase to the solid phase. Adsorption process occurs on the surface of adsorbent material [21]. Biosorption is an important technique to remove toxic metals from aqueous media and organic pollutants due to its simplicity, efficiency and cost-effectiveness. In adsorption, substances are bound through physical or chemical interactions to solid surface. Hence, it is a mass transfer process and an efficient method for the treatment of effluents. Several low-cost adsorbents have been derived from industrial processes, agricultural waste, natural products, or different biopolymers and activated carbon and applied to remove toxic metal ions from polluted or contaminated water.

Saccharum munja plant is used to reduce thirst, dyspraxia, burning sensation and urinary complaints. In many places are abundantly found and thus could be used as potential sources of metabolites and bioactive compounds [22]. We have used *Saccharum munja* plant as an efficient adsorbent to produce biochar and novel nanomaterial to carry out adsorption experiments and equilibrium study. The purpose of the study was to elaborate effectiveness of adsorption process with minimum amount of nano material adsorbents for the removal of metals on large scale. Adsorption kinetics are helpful to give favorable results about adsorption mechanisms by using controlling conditions. The pseudo first order models are applied to study biosorption of sorbate on the biosorbents. Rate limiting reaction follows chemisorption in PSO II model. Energy and conversion of energy in different forms is studied under thermodynamics. In thermodynamics, different transformations are made in different systems. Thermodynamic parameters determine spontaneity of a process. These parameters include enthalpy change ($\Delta H°$), free energy change ($\Delta G°$) and entropy change ($\Delta S°$). As temperature increases, value of $\Delta G°$ and $\Delta H°$ decrease.

Materials and Methods

Screening and Treatment of Adsorbent

Different adsorbent materials like almond shell, coconut shell and *Saccharum munja* stem were screened through batch adsorption experiments for selection of best adsorbent. For this purpose sorbents were washed, dried and ground to suitable sieve size. In order to select feedstock with good metal removal efficiency, batch sorption experiments were performed to remove initially Cr(III) metal from aqueous solution. For this purpose, 1 g of each biomass was treated with 100 ml of 60 ppm solution of chromium, taken in 250ml conical flask and stirred at orbital shaker with 150rpm speed for 1 h. Atomic absorption spectrophotometer having model no. AA-6300 SHIMADZU, JAPAN was used to analyze these filtered solutions. A comparison was made on sorption potential of these sorbents and *saccharum munja* was selected, as favorable sorbent for further experimental work and analysis.

Preparation of Biochar and Formation of Hematite Nanoparticles

Saccharum munja biomass was ground to fine powder of desired mesh size and biochar was prepared through pyrolysis by taking biomass in a crucible that was covered with lid. For this pyrolysis process, a furnace was used whose temperature was kept constant at 450°C for almost one hour. Crucibles were cooled at room temperature to get *Saccharum munja* biochar (SMBC). Hematite loaded *Saccharum munja* biochar nanoparticles were prepared by using freshly prepared iron chloride ($FeCl_3$) solution. A suspension of biochar was made in distilled water and stirred by mixing with iron chloride solution. pH adjustment upto 11 was made with addition of 0.1 M sodium hydroxide solution. Upon continuous shaking for 1 h and drying treatments hematite based nanomaterial was obtained and named as HLSMBC (hematite loaded *saccharum munja* biochar) [23].

Characterization

Characterization of sorbent materials was important for identification of structural surface adsorption properties, owing to presence of functional groups like hydroxyl, nitro, carbonyl etc. For this purpose two techniques SEM for analysis of surface morphology and FTIR for surface activated groups were used.

Adsorption Experiments

In case of adsorption of chromium, batch wise adsorption experiments were performed using standard solutions of chromium prepared from chromium oxalate salt. 15-90 ppm solutions were tested through experiments for 1g of each adsorbent at orbital shaker with agitation speed of 150 rpm at room temperature. Flasks were filtered and filtrate were analysed with atomic absorption spectrophotometer. Cr(III) sorption was observed with three forms of *Saccharum Munja* sorbent (SM, SMBC, and HLSMBC).

The amount of metal adsorbed on adsorbent and sorption efficiency were calculated using concentration at equilibrium as:

$$q_e = V (C_0-C_e)/W \quad (1)$$

$$\% \text{ removal} = C_0-C_e/C_0 \text{ x}100 \quad (2)$$

C_0 (g/L), initial conc. of metal ion, C_e, equilibrium con. Of metal ion, V as metal solution volume in liter, and W, weight of sorbent (g).

Adsorption Isotherms

Adsorption equilibrium studies are examined through isotherm models to ensure adsorbent and sorbate interaction. These isotherms are used to give results of best fit of data, and are named as Dubinin , Temkin, Langmuir, Freundlich, Halsy, Toth, Sips and Redlich-Peterson.

Linear and Non-Linear Sorption Models Analysis

To describe experimental parameters in isotherms linear regression analysis is used. It shows a relationship among amount of sorbate and its concentration at equilibrium. Errors that results from linear regression analysis of linear forms of isothermal data can be eliminated by non-linear regression analysis, as an efficient tool. Non-linear analysis is now used in many applications such as effluents treatment, waste water etc [24].

Langmuir Isotherm Model

Langmuir isotherm is described most commonly by the formation of a monolayer of sorbate on the surface of sorbent with on side way interactions. Earlier, it was used to describe adsorption of gas and solid phase, later it was also used to explain a comparison among sorption efficiency of various sorbents [25]. Adsorption data is described in this isotherm by linear and non-linear analysis.

$$\text{Linear form} \qquad (Ce /q_{eq}) = (Ce /q_{m)+} (1/ b \text{ x } q_m) \quad (3)$$

$$\text{Non-linear form} \qquad q_{eq} = q_m b C_e/1+ b C_e \quad (4)$$

Langmuir isotherm plot among Ce & Ce/qe gives data information about Langmuir constants and adsorption reaction rates. These plots are designed to check whether adsorption is favorable or not.

Freundlich Isotherm Model

Freundlich isotherm is described by the formation of a multilayer of sorbate on heterogeneous surfaces of sorbent. In this isotherm adsorption data is best described at low

concentrations [26]. Also, for comparison of adsorption mechanism, linear and non-linear analysis is performed to get best fitted results.

$$\text{Linear form} \quad \ln (q_{eq}) = \ln K_F + (1/n) \ln (C_e) \quad (5)$$

$$\text{Non-linear form} \quad q_{eq} = K_F C_e^{1/n} \quad (6)$$

q_e shows amount of sorbate which is adsorbed per unit mass of the sorbent surface, Ce represents concentration of sorbate at equilibrium. K_F constant shows capacity of adsorbent for adsorption and n is adsorption feasibility constant and they can be obtained from intercept of slope.

Dubinin-Radushkevich Isotherm Model

Adsorption mechanism is also described by Dubinin-Radushkevich isotherm for porous adsorbents with heterogeneous surfaces. Adsorption data is fitted to show maximum adsorption of solute and Gibbs free energy distribution [27]. The model favours only intermediate concentrations or sorbate and in some cases give unrealistic results and low values [28].

$$\text{Linear form} \quad \ln q_e = (\ln q_s) - K_{ad} \varepsilon^2 \quad (7)$$

$$\text{Non-linear form} \quad q_e = (q_s) \exp(-K_{ad} \varepsilon^2) \quad (8)$$

q_e is the amount of adsorbate (mg/g) on adsorbent, q_s is saturation capacity and K_{ad} is constant which shows physical and chemical adsorption at intermediate concentrations data. Ɛ is Polanyi potential.

Temkin Isotherm Model

Adsorbate-adsorbent interactions are studied in Temkin isotherm model by ignoring initial and final concentration values.

$$\text{Linear form} \quad qe = RT/\Delta Q \ln K_0 + RT/\Delta Q \ln C_e \quad (9)$$

$$\text{Non-linear form} \quad qe = RT/\Delta Q \ln K_0 C_e \quad (10)$$

In linear and non-linear forms T represents temperature (°C or K), R, universal constant (j/mol.K), qe amount adsorbed and Ce equilibrium concentration. K_0 is Temkin model constant.

Elovich Isotherm Model

Elovich isotherm represents multilayer coverage of adsorbent surface with metal ion or other adsorbate species. With an assumption to cause an exponential increase in sorption process. It explains chemisorption process [29].

$$\text{Linear form} \quad \ln q_e/C_e = \ln K_E Q_m - q_e/Q_m \quad (11)$$

$$\text{Non-linear form} \quad q_e/Q_m = K_E C_e \exp q_e/Q_m \quad (12)$$

The plot indicates value of maximum sorption capacity and Elovich constant with a graph among qe and $\ln q_e/C_e$.

Error Function Analysis

For error function analysis linear and non-linear error equations were applied on adsorption results. These error equations predict feasibility of isotherms and named as Average relative error, Sum Square of errors, Sum of absolute error, chi-square test, Coefficient of determination and Average percentage error.

Kinetic Study

Kinetic studies reveal tendency of adsorption process over time. Sorption shows a dynamic mechanism to evaluate rate of reaction with time in the range of 10-70 mint. For 100ppm chromium solution. All solutions were shaken onto orbital shaker at speed of 150 rpm and filtered solutions were kept for analysis through AAS. These experimental results were used to equate PFO I and PSO II models.

Thermodynamic parameter

Temperature parameters were optimized for thermodynamic investigations in the range of 293-328K. For uptake of lead on all three forms of adsorbent, 1g of each adsorbent was shaken at desired temperature range. After calculation of experimental results, they were applied on adsorption thermodynamic equations to find out entropy change, free energy change and enthalpy change.

Results and Discussion

Equilibrium experiments that were performed for remediation of chromium from aqueous media, evaluated the results for various factors followed by adsorbents structural characterization.

Adsorbents characterization

SEM working is fast, affordable and easy for trained workers with advanced computer systems and software. It provide different signals with multiple detectors, and digital image of sample with minimum preparation and less time. [30, 31]. Sorbents were characterized through scanning electron microscope, and images suggested an improved surface roughness and tubular ways for maximum metal binding on its surface.

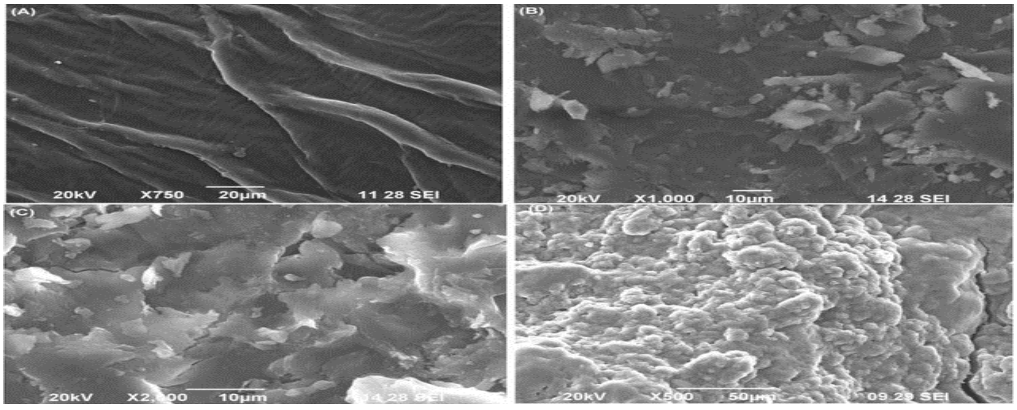

Fig. 1. SEM image (A) of raw SM, (C) of SMBC and (B & D) of HLSMBC [23]

FTIR spectra is plotted using transformation process of converting raw results into a spectrum [32]. Functional sites on nanostructure surface can be determined under specific conditions. So, the groups responsible for adsorption can be identified [33]. Fourier transform infrared spectra were taken for all adsorbents prior to and after metal adsorption. These spectra proved presence of different functional groups, which were responsible for chromium adsorption. There was a change in all forms of spectra. FTIR spectra of raw munja and its biochar are given. –OH peaks in the range of 3000-3500 cm^{-1} for raw munja and SMBC, but prominent effects were observed for biochar form of adsorbent. Nitro stretching peaks were observed at 1300-1450 cm^{-1} with highest peak for HLSMBC. Hydroxyl group peak was observed at 3287 for uptake of chromium. Peaks at 1700-1725 cm^{-1} showed presence of carboxyl or carbonyl groups. Moreover, peaks at 1480-1600 cm^{-1} shows aromatic groups and for C-N group peaks appear at 1000-1250

cm^{-1}. FTIR of raw HLSMBC is compared with IR for removal of chromium by HLSMBC. Fe-O peak is observed in (567)500-600 range, which is responsible for metal removal along with –OH bending vibrations. CH- stretch follows the range of 2850-2990. –OH stretching vibrations appear in the range of 3200-3700 and causes adsorption of metal on nanomaterial by involving –OH group.

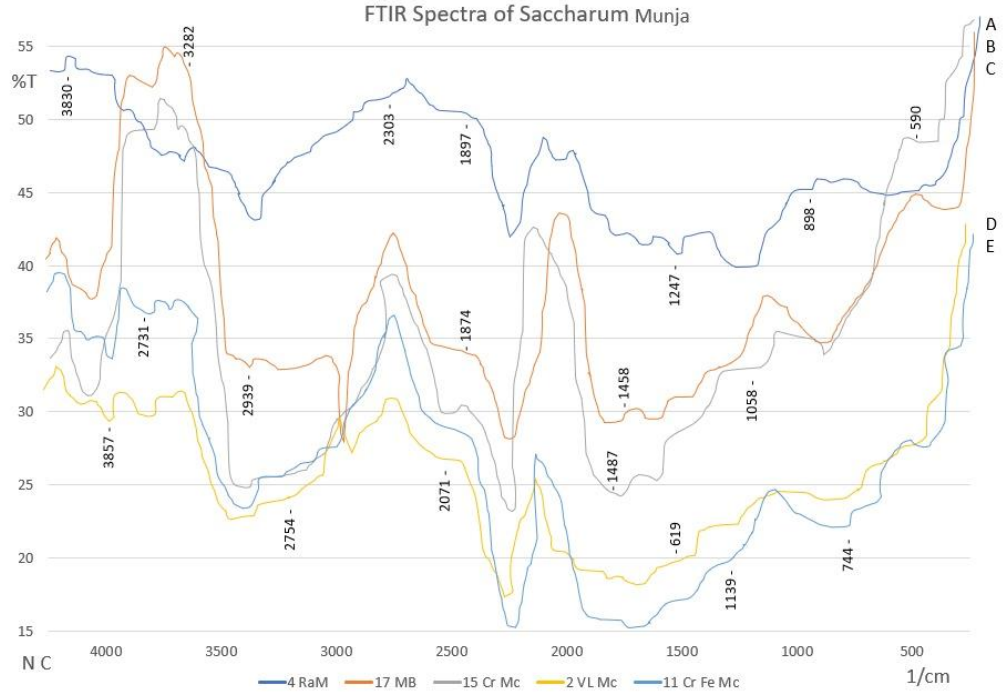

Fig. 2. (a) FTIR spectra of Raw SM (*saccharum munja*) (b) SMBC (*saccharum munja* biochar) (c) SMBC after adsorption of chromium d. HLSMBC (Hematite loaded *saccharum munja* biochar) (e) HLSMBC (Hematite loaded *saccharum munja* biochar) after adsorption of chromium

Adsorption Studies

Chromium adsorption on SM, SMBC and HLSMBC was observed as a function of experimental parameters. The results indicate that when the concentration is increased from 15-90 ppm the adsorption capacity of Cr(III) metal on sorbents is increased. Adsorption experiments for chromium removal revealed an increase in adsorption with an increase in metal concentration. So higher concentration facilitated the adsorption of metal on adsorbents surface. It is evident that adsorbents can remove metal at higher metal concentrations, indicating availability of more functional groups on their surface for metal binding in Figure 3. Raw form of SM exhibits more sorption capacity as compared to SMBC showing variation of water molecules and functional groups on their surfaces. But hematite loaded sorbent showed increase in adsorption capacity at high concentration, showing availability of surface sites on nanomaterial sorbent.

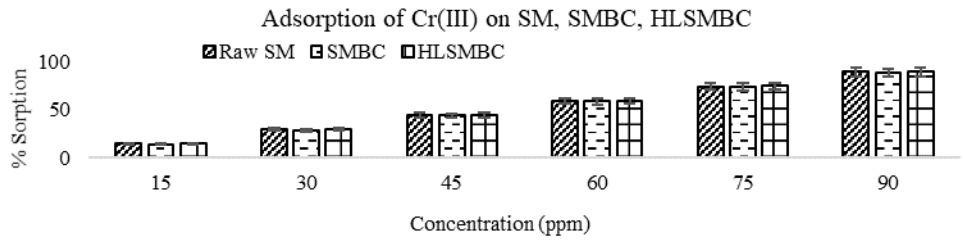

Fig. 3. Comparison among three forms (raw SM, SM biochar & Hematite loaded SMBC) of *Saccharum munja* biosorbents for adsorption of Chromium(III) upon variation in concentration (ppm)

Adsorption Isotherm Models

Langmuir, Freundlich, Dubnin-Radushkevich, Elovich and Temkin isotherms had been applied on equilibrium adsorption data. For this purpose linear and non-linear equations were used to evaluate experimental findings.

Freundlich Isotherm

Freundlich isotherm is applied on adsorption data to find out constants K_F and n. where K_F is maximum adsorption capacity of adsorbent, whose high value shows high adsorption on adsorbent surface. High value of correlation coefficient R^2 shows more adsorption process. Positive value of n suggests favorable process while negative value shows unfavorable process. Freundlich plots for chromium adsorption are shown below. These plots favours this isotherm owing to good R^2 values and favorable values of constants. R^2 =0.9363 for SM shows best removal of chromium through multilayer adsorption. Also high value of K_F suggest maximum adsorption of chromium on this form. SMBC and HLSMBC also indicated favorable values of R^2 and followed this isotherm. Values of non-linear forms of Freundlich constants are also given in table. 1. Adsorption results revealed good results for Freundlich isotherm in uptake of chromium. Constants n & K_F values were calculated from intercept and slope of the graph favoring high adsorption process rate of chromium adsorption onto sorbates surfaces. Freundlich plots indicating chromium removal are shown below. These plots favours this isotherm owing to good R^2 values and favorable values of constants. Values of non-linear forms of Freundlich constants are also given in Table 1, which also follows experimental results.

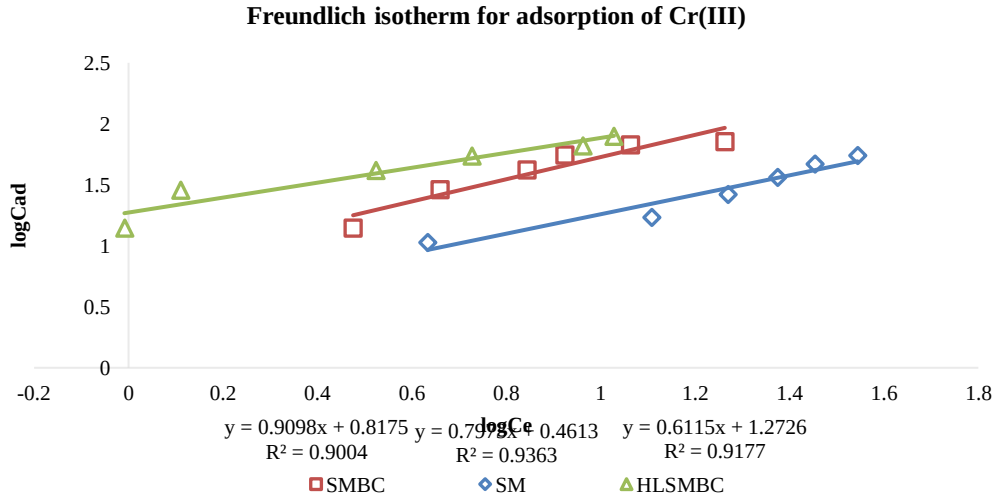

Fig. 4. Freundlich isotherm for removal of Cr(III)

Table 1. Freundlich constants for uptake of chromium on three adsorbents

Adsorbents	Adsorbate	Freundlich linear results			Freundlich Non-Linear results	
		K_f constant	n constant	R^2 values	K_f constant	n constant
Saccharum munja	chromium	2.892677	1.254233	0.9363	0.2	0.218
***Saccharum munja* BC**		20.97008	1.724138	0.9004	0.13	0.258
HL *Saccharum munja* BC		18.73268	1.635323	0.9177	1.99	2.34

Langmuir Isotherm

Results for Langmuir model are shown in table. Langmuir model facilitates monolayer sorption of sorbate on sorbent surface. From equation Langmuir constants Q_0 and b were calculated. Q_0 is maximum monolayer adsorption capacity and intensity of sorption process depends upon high surface capacity of adsorbent medium as well as its sieve size. Experiments performed with 15-90 ppm solutions of sorbate and 1 g of sorbents and Langmuir model was applied on results. Coefficient R^2 results were calculated from Langmuir graph as given in table 2. Which reveals high value of correlation coefficient in case of hematite loaded adsorbent with high sorption.

Langmuir constant Q_0 values are increased with an increase in adsorption process. These constants are calculated from slope and intercept of isotherm. For chromium removal Langmuir plots and their values are also shown. It is clear that only HLSMBC support Langmuir isotherm following monolayer sorption but all other sorbents did not support isotherm due to small values of R^2 and negative values of Q_0 and b. Negative constant values give the fact that adsorption conditions for these sorbents are different from those assumed for Langmuir isotherm [34].

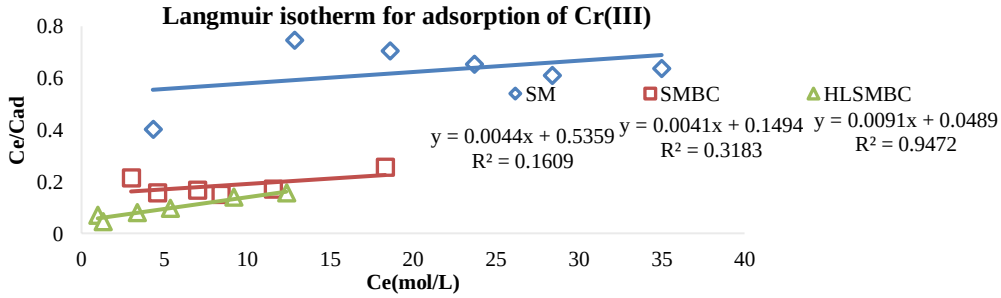

Fig. 5. Langmuir isotherm for removal of Cr(III)

Table 2. Langmuir constants for uptake of chromium on three adsorbents

Adsorbents	Adsorbate	Linear Langmuir results			Non-Linear Langmuir results	
		Q_0 value	b value	R^2 value	Q_0 value	b value
Saccharum munja	Cr(III)	227.27	0.00821	0.1609	68.98	0.067
***Saccharum munja* BC**		243.90	0.02744	0.3183	56.43	0.098
HL *Saccharum munja* BC		109.89	0.1861	0.9472	43.8	0.13

ELOVICH ISOTHERM

Elovich isotherm plots are also given with R^2 in the order 0.7124 (HLSMBC) > 0.1126 (SM) > 0.0215 (SMBC), indicating poor fit of chromium adsorption into Elovich model for

HLSMBC, SM and SMBC. Linear and non-linear values of Elovich constants are given in table. High values of these constants supports model and low values indicate poor fit.

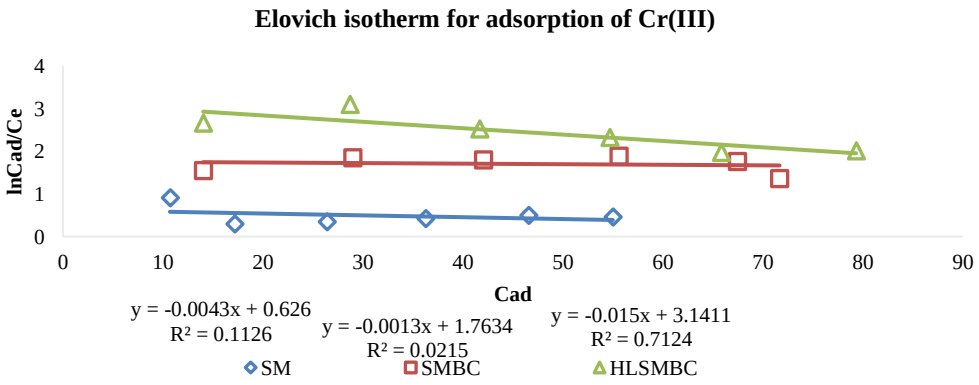

Fig. 6. Elovich isotherm for removal of Cr(III)

Table 3. Elovich constants for uptake of chromium on three adsorbents

Adorbents	Adsorbates	Elovich linear form			Elovich Non-Linear form	
		Constant K_e	Adsorption capacity Q_m	R^2	Constant K_e	Adsorption capacity Q_m
Saccharum munja	Cr(III)	0.0080	232.55	0.1126	0.0027	675.3
***Saccharum munja* BC**		0.0075	769.23	0.0215	0.007	295.7
HL *Saccharum munja* BC		0.3469	66.66	0.7124	0.0034	899

Dubinin-Radushkevich Isotherm

Dubinin-Radushkevich isotherm permits adsorption onto heterogeneous multilayer surfaces of sorbent, depending on temperature changes. The model was applied to study physical and chemical sorption of chromium onto different forms of adsorbents surfaces. R^2 value and constants values qs and Kads were obtained from slope and intercept by plotting ln Cad and Ɛ2. Plot among adsorption capacity and adsorption concentration gives Dubinin-Radushkevich isotherm. Linear plot is formed for adsorption of chromium onto SM, SMBC and HLSMBC, and isothermal parameters were tabulated. The coefficient readings are in the range of 0.9729 > 0.9272 > 0.653, indicating best fit of data with Dubinin isotherm.

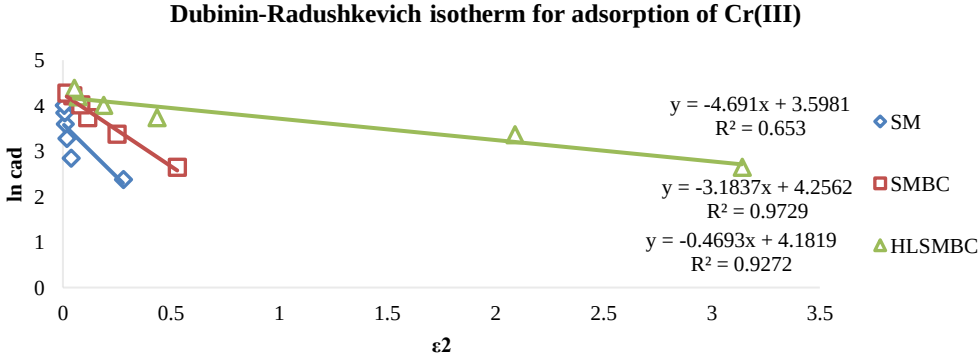

Fig. 7. Dubinin-Radushkevich isotherm for removal of Cr(III)

Table 4. Dubinin-Radushkevich constants for uptake of chromium on three adsorbents

Adsorbents	Adsorbates	Dubinin-Radushkevich linear results			Dubinin-Radushkevich Non-Linear results	
		Constant Kads	Constant qs	Value of R^2	Constant Kads	Constant qs
Saccharum munja	Cr(III)	-4.691	36.52	0.653	-0.34	23
***Saccharum munja* BC**		-3.1837	70.54	0.9729	-0.25	24
HL *Saccharum munja* BC		-0.4693	65.49	0.9272	-0.9	65.4

Temkin Isotherm

Temkin isotherm assumes that surface coverage is enhanced with an increase in adsorption process. It also suggested a linear plot for heat of adsorption. Temkin constants were calculated from slope and intercept of linear and non-linear plots obtained from respective isotherm equations. Results of adsorption experiments were used to find fit of chromium adsorption into linear and non-linear form of Temkin isotherm. R^2=0.9611 for SMBC, 0.9622 for HLSMBC showed favorable adsorption and best fit for Temkin isotherm. Adsorption heat constant values are B= 34.12 > 23.75 > 20.36 for SMBC > HLSMBC > SM in linear model. Heat energy adsorption constant K_t values are also given, in the range of 0.28-2.03 also reveals favorable data for isotherm (Table. 5). For nonlinear data kt, constant values are in the range of 0.18-0.63, and B values are in the range of 19.2-27.3 which follows requirements of Temkin isotherm.

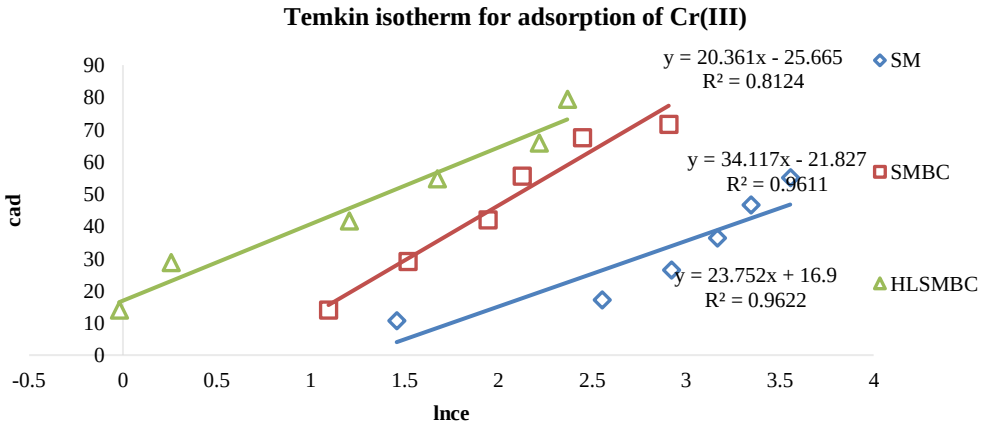

Fig. 8. Temkin isotherm for removal of Cr(III)

Table 5. Temkin constants for uptake of chromium on three adsorbents

Adsorbents	Adsorbates	Linear form of Temkin isotherm			Non-Linear form of Temkin isotherm	
		Constant K_t	Constant B	Value of R^2	Constant K_t	Constant B
Saccharum munja	Cr(III)	0.28	20.36	0.8124	0.63	19.2
***Saccharum munja* BC**		0.53	34.12	0.9611	0.18	21.98
HL *Saccharum munja* BC		2.03	23.75	0.9622	0.57	27.3

R^2 value for *Saccharum munja* was high in Freundlich isotherm, for *Saccharum munja* biochar it was large in Dubinin-Radushkevich and in case of Hematite loaded *Saccharum munja* high value was obtained for Temkin.

SM, R^2= Freundlich (0.9363) > Temkin (0.8124) > Dubinin-Radushkevich (0.653)> Elovich (0.1126) > Langmuir (0.1609)

SMBC, R^2 = Dubinin-Radushkevich (0.9729) > Temkin (0.9611) > Freundlich (0.9004) > Langmuir (0.3183) > Elovich (0.0215)

HLSMBC, R^2= Temkin (0.9622) > Langmuir (0.9472) > Dubinin-Radushkevich (0.9272) > Freundlich (0.9177) > Elovich (0.7124)

Error Analysis

Error distribution for equilibrium experimental results for chromium adsorption was calculated for all isotherms in linear and non-linear forms. Error data is given in table and comparison among isotherms errors is shown below to find the best fit results.

Error Analysis

In case of SM adsorption, for linear approach Langmuir and Dubinin-Radushkevich isotherms data showed least error values followed by Elovich model. For non-linear approach Langmuir and Elovich error values revealed less values to follow equilibrium adsorption results. Freundlich and Temkin isotherms showed high values of errors to unfollow equilibrium data. For adsorption through SMBC, error analysis for removal of chromium showed that Temkin RSS error has lowest value, Freundlich EABS, Langmuir chi square and Dubinin-Radushkevich APE has lowest values to count for adsorption data. For non-linear form Langmuir showed least RSS, APE, Freundlich EABS, and Temkin chi-square to support adsorption experimental results. Calculation of error function for HLSMBC showed least errors for Langmuir and Dubinin-Radushkevich isotherms which minimizes the error distribution among data. For non-linear approach Elovich and Langmuir models gave small values followed by Freundlich isotherm.

Table 6. Error function values calculated from isothermal data of SM experiments

Error names	Sum square of errors	Sum of absolute error	Chi -square error	Average percentage error	Average relative error
Linear isotherms					
Freundlich	0.0234	4.0127	3.1705	4.2794	0.060
Langmuir	-0.0035	-0.0035	0.0035	0.1991	-0.199
Elovich	$8.53*10^{-6}$	-0.0029	0.8180	-13.634	-4.9082
Dubinin-Radushkevich	11.035	-3.322	3.0982	-23.022	-8.288
Temkin	$5.21*10^{-5}$	0.0072	0.0200	-0.1203	-0.1203
Non-Linear isotherms					
Freundlich	$1.05*10^{-7}$	0.0007	0.0003	47929	4.889
Langmuir	-0.0033	3.747	-3.4772	-5.992	5.992
Elovich	$1.1*10^{-12}$	$-1.04*10^{-6}$	-6.000	$1.27*10^{-6}$	$4.57*10^{-7}$
Dubinin-Radushkevich	$1.37*10^{-5}$	0.0036	$-4*10^{-7}$	-0.0085	-0.0030
Temkin	0.00055	0.02364	-38.420	-0.3941	230.52

Table 7. Error function values calculated from isothermal data of SMBC experiments

Error names	Sum square of errors	Sum of absolute error	Chi -square error	Average percentage error	Average relative error
Linear isotherms					
Freundlich	0.3609	-147.10	109.45	2.9405	-2.24
Langmuir	0.0018	0.0018	-0.0018	0.1425	-0.1425
Elovich	$6.85*10^{-5}$	-0.0082	0.0834	-1.3904	-0.5005
Dubinin-Radushkevich	43.311	-6.5811	5.2392	-36.019	-12.967
Temkin	$1.38*10^{-5}$	0.0037	0.1067	-0.0619	-0.6403

Non-Linear isotherms					
Freundlich	$1.01*10^{-6}$	0.0022	0.0020	32933	60.36
Langmuir	-0.0001	1.1120	-1.1120	-5.986	5.986
Elovich	$1.15*10^{-10}$	$1.07*10^{-5}$	-6.000	$-1.4*10^{-5}$	$-5.1*10^{-6}$
Dubinin-Radushkevich	2.89*10-5	0.0053	-8.5*10-7	-0.0130	-0.0046
Temkin	0.0002	0.0151	-17.025	-0.2522	102.15

Table 8. Error function values calculated from isothermal data of HLSMBC experiments

Error names	**Sum square of errors**	**Sum of absolute error**	**Chi -square error**	**Average percentage error**	**Average relative error**
Linear isotherms					
Freundlich	0.0313	0.2465	4.0255	2.9374	0.084
Langmuir	-0.0013	-0.0013	0.0013	0.1509	-0.1509
Elovich	$7.82*10^{-5}$	0.0088	0.0343	-0.5732	-0.2063
Dubinin-Radushkevich	31.408	-5.604	4.5529	-31.511	-11.344
Temkin	$5.51*10^{-6}$	-0.0023	0.0779	0.0391	-0.4679
Non-Linear isotherms					
Freundlich	$1.06*10^{-6}$	0.00230	0.0020	3289	80.90
Langmuir	0.0009	0.5647	-0.5647	-5.985	5.985
Elovich	$1.59*10^{-11}$	$3.98*10^{-6}$	-6.000	$-4.8*10^{-6}$	$-1.7*10^{-6}$
Dubinin-Radushkevich	$2.99*10^{-5}$	0.0054	$-9*10^{-7}$	-0.0132	-0.0047
Temkin	0.0002	0.0142	-14.657	-0.2373	87.945

Kinetic Models

A relationship among time and quantity of adsorbate specie onto adsorbent surface describes kinetics [35]. PFO and PSO models were applied on experimental findings to calculate rate of reaction for adsorption of metal by changing time factor experiments. These calculations were than used to draw graph among parameters. All results were than elaborated in the form of figures and tales.

Kinetic Models for Cr(III) Adsorption onto Raw Sm

Uptake of chromium by raw SM was also studied through adsorption experiments as a function of time. Plot for PFO and PSO are given and kinetic parameters calculated from the graph are written in table. R^2=0.9866>0.6443 for PSO I >PFO clearly indicates that PSO I strongly supports adsorption than PFO. Poor relation of PFO suggests that only PSO favours adsorption of chromium onto SM through ion exchange process.

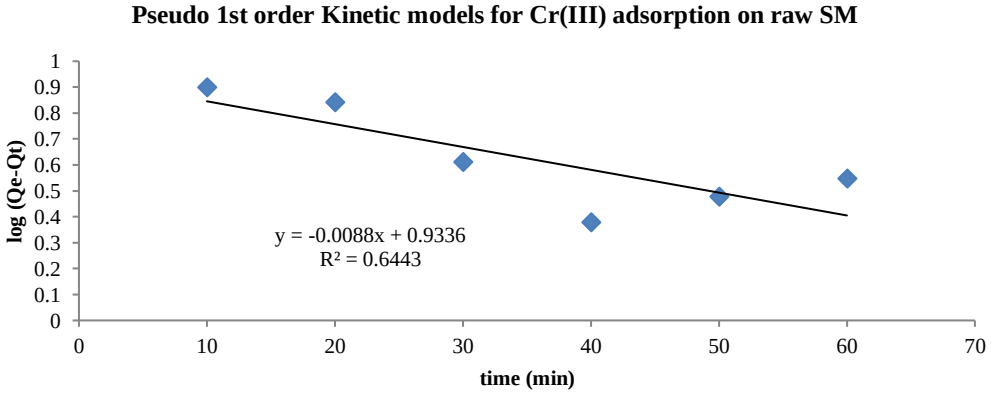

Fig. 9. Pseudo first order (PFO) kinetic model showing Plot among log (Qe-Qt) vs t (min) for adsorption of Cr(III) on SM

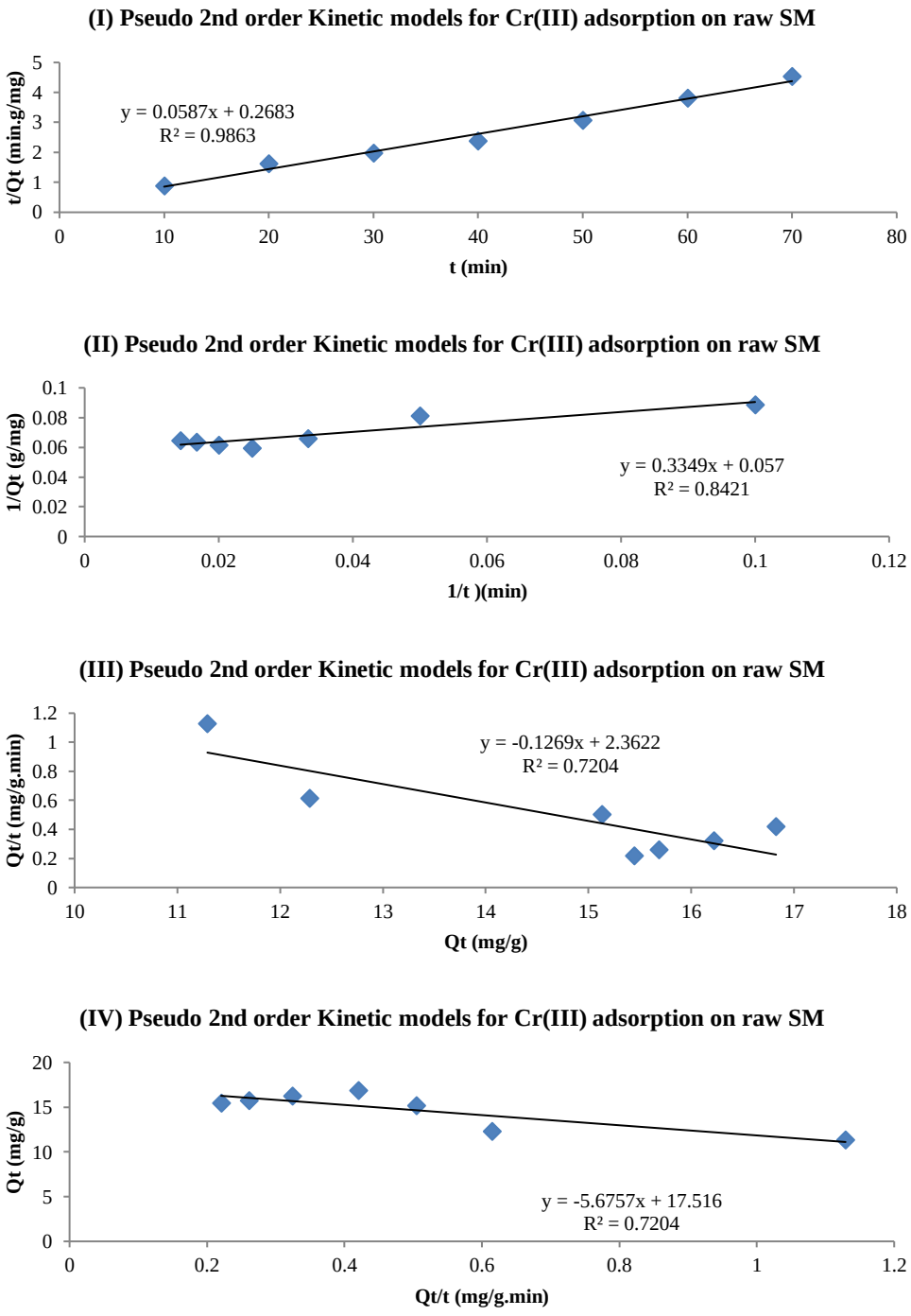

Fig. 10. Pseudo second order kinetic model showing adsorption of Cr(III) on SM: a) (Type I) Plot among t/Qt vs t (min); b) (Type II) plot among 1/Qt vs 1/t (min); c) (Type III) Plot among Qt/t vs Qt; d) (Type IV) Plot among Qt vs Qt/t

Table 9. PFO and PSO calculations for uptake of chromium by SM adsorbent, **a.** SM adsorbent

Kinetic Parameters of chromium adsorption by SM				
PSO model	**Parameters of PSO calculations**			
	R^2	**k constant**	**Values of Qe**	**h constant**
Type I	0.9863	0.0128	17.03	3.72
Type II	0.8421	0.0097	17.54	2.98
Type III	0.7204	0.0068	18.61	2.36
Type IV	0.7204	0.0100	17.51	3.08
PFO model	**R^2**	**k**		
	0.6443	-0.0088		

SMBC

To study the removal of chromium removal by SMBC PFO and PSO both the models have high R^2 value i.e. PFO R2=0.9958, PSOI R2=0.9963~1 suggesting physicochemical adsorption of chromium onto SMBC. Qe=19.88 and k=0.0193, h=2.77 for PSO I shows greater adsorption of chromium than PFO.

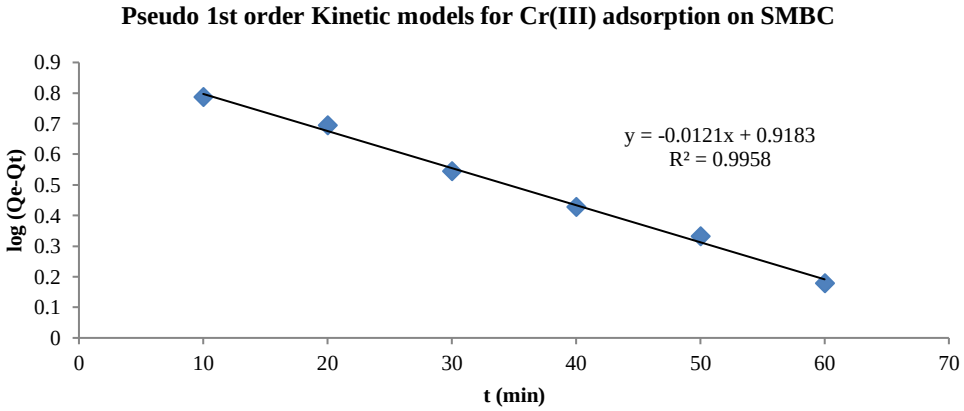

Fig. 11. Pseudo first order (PFO) model showing graph among log (Qe-Qt) vs time (min) for adsorption of Cr(III) on SMBC

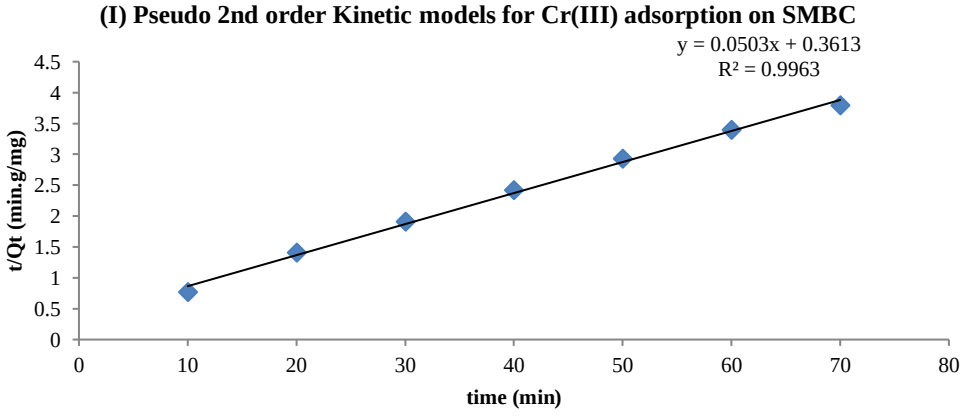

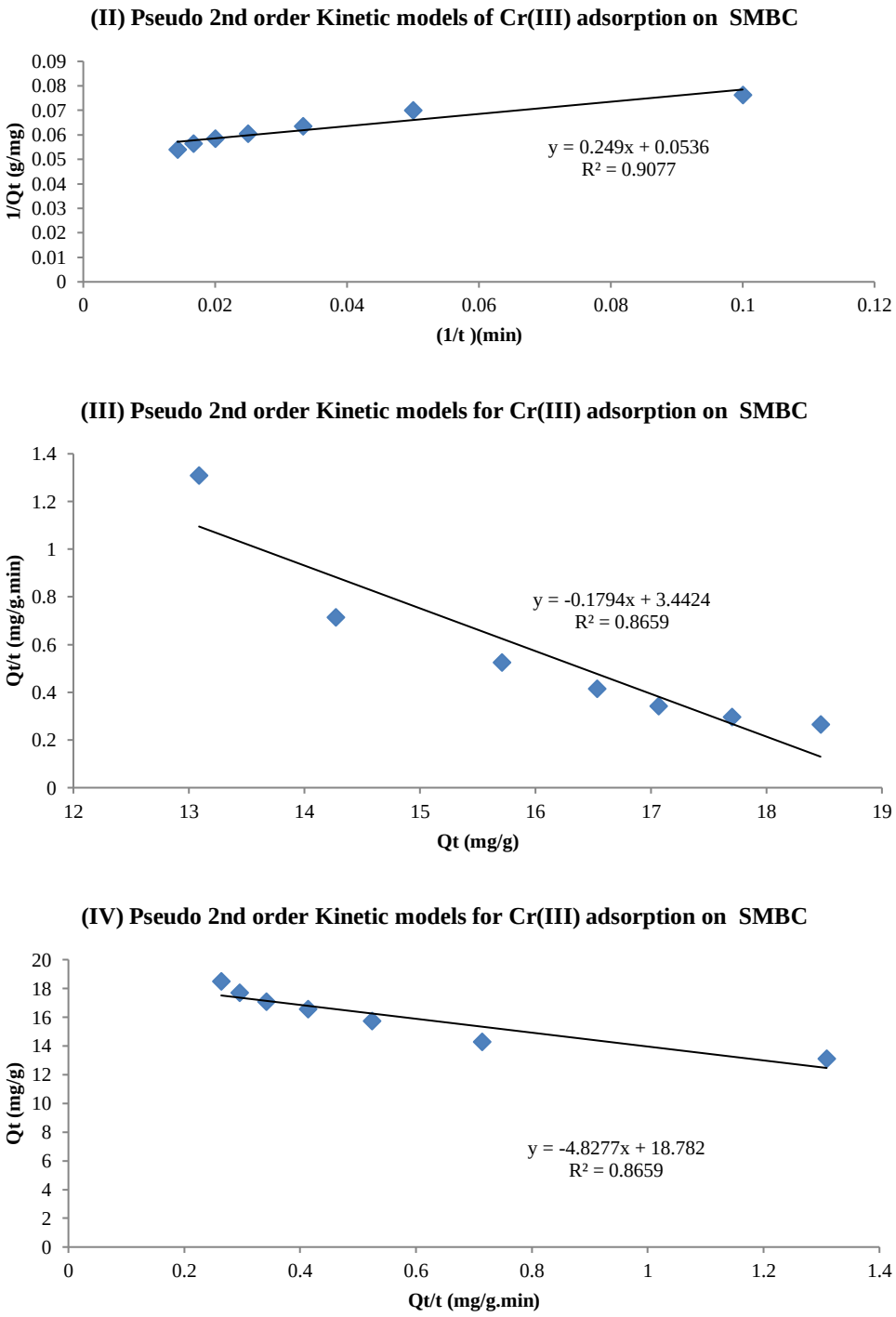

Fig. 12. Pseudo second order kinetic model showing adsorption of Cr(III) on SMBC: a. (Type I) Plot among t/Qt vs t (min); b. (Type II) plot among 1/Qt vs 1/t (min); c. (Type III) Plot among Qt/t vs Qt; d. (Type IV) Plot among Qt vs Qt/t

Table. 9 b. SMBC Adsorbent

Kinetic parameters of chromium adsorption by SMBC				
PSO model	**Parameters of PSO calculations**			
	R^2	**k constant**	**Value of Qe**	**h constant**
Type I	0.9963	0.0193	19.88	2.77
Type II	0.9077	0.0115	18.65	4.01
Type III	0.8659	0.0093	19.18	3.44
Type IV	0.8659	0.0110	18.78	3.89
PFO model	**R^2**	**k**		
	0.9958	0.0121		

HLSMBC

Chromium adsorption experiments with change in time were performed and kinetic study was observed from plot of PFO and PSO models. PSO coefficient has value 0.9997 greater than PFO coefficient value 0.9928, and both the models favours adsorption process indicating single and double sites occupation of adsorbate on adsorbent surface. Qe has maximum value i.e. 20.08 for PSO and k_2 value 0.0114 lesser than other value, assuming better fit of PSO I model.

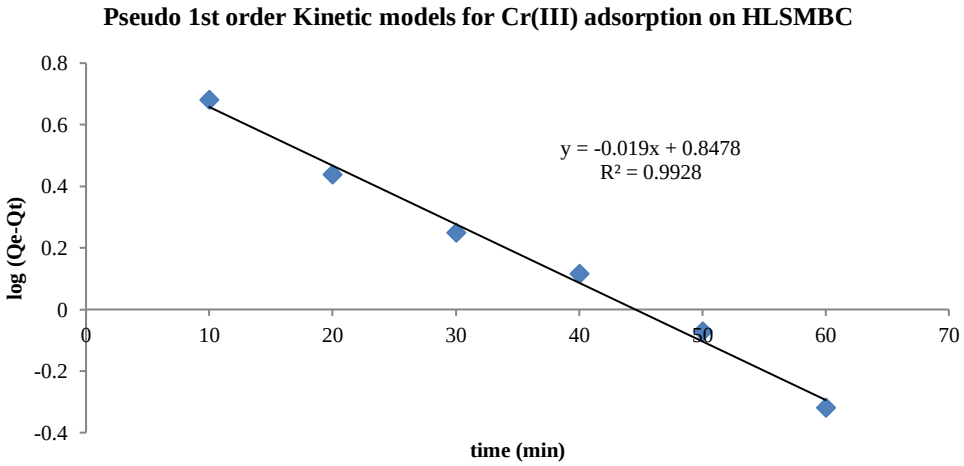

Fig. 13. Kinetic calculations for PFO model showing results of graph among log (Qe-Qt) vs time (min) for adsorption of Cr(III) on HLSMBC

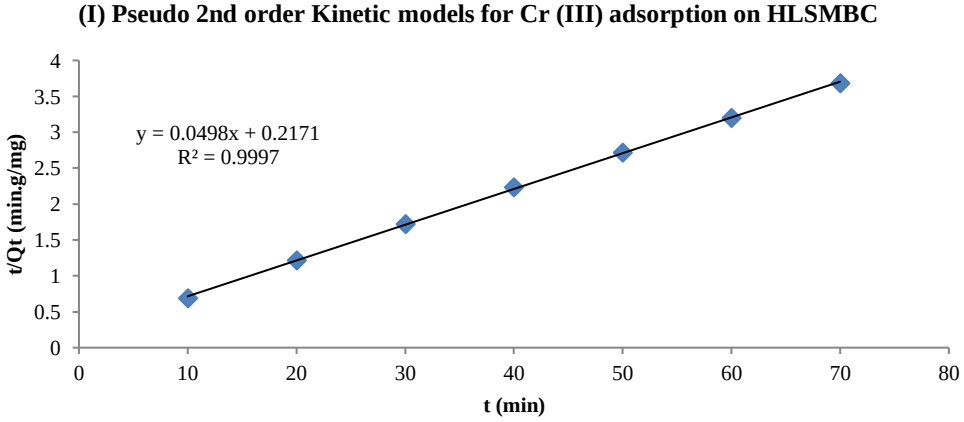

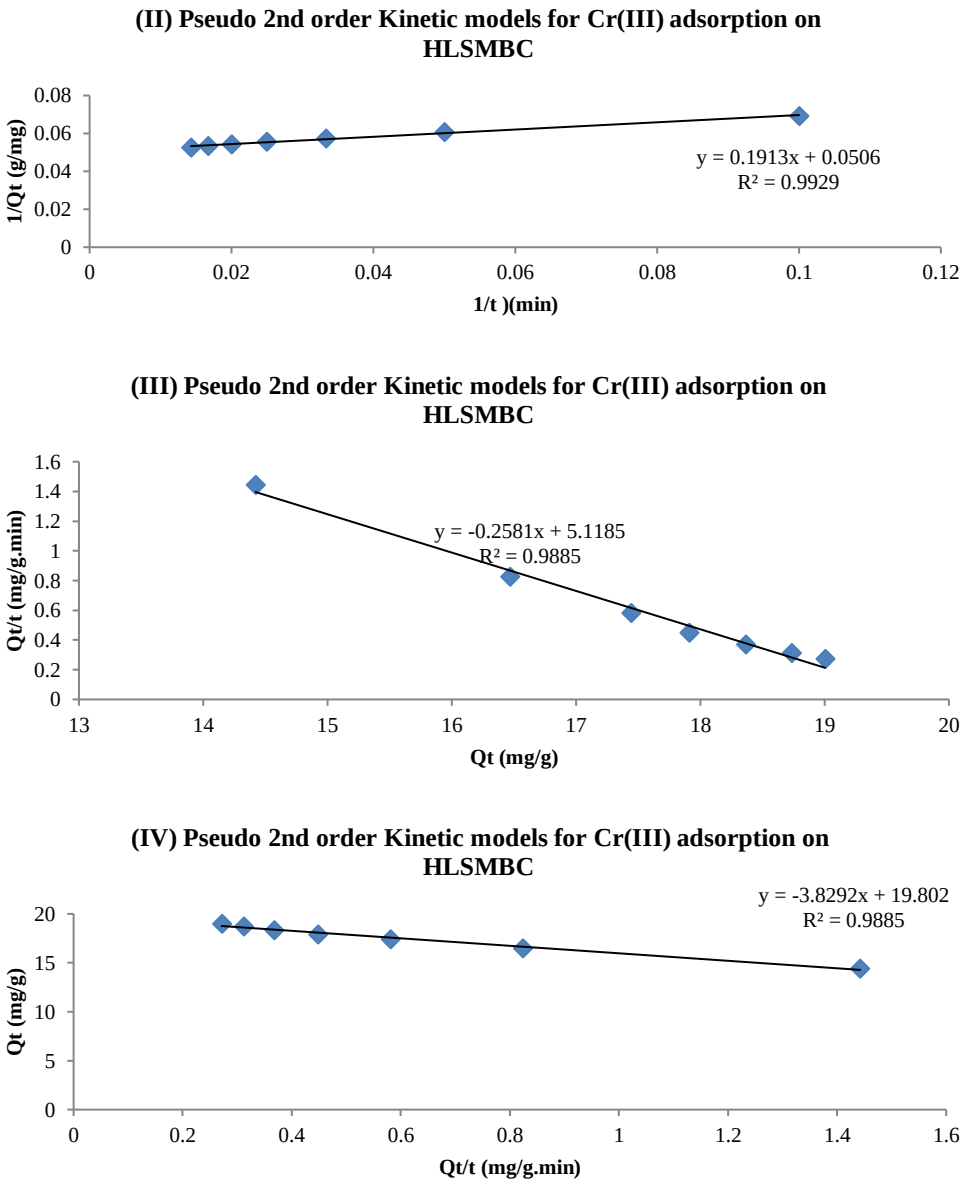

Fig. 14. Pseudo second order kinetic model showing adsorption of Cr (III) on HLSMBC: a. (Type I) Plot among t/Qt vs t (min); b. (Type II) plot among 1/Qt vs 1/t (min); c. (Type III) Plot among Qt/t vs Qt; d. (Type IV) Plot among Qt vs Qt/t

Table 9 c. HLSMBC adsorbent

Kinetic parameters of chromium adsorption by SMBC

PSO model	**Parameters of PSO calculations**			
	Value of R^2	**Constant k**	**Value of Qe**	**h constant**
Type I	0.9997	0.0114	20.08	4.60
Type II	0.9929	0.0133	19.76	5.22
Type III	0.9885	0.0130	19.83	5.11
Type IV	0.9885	0.0131	19.80	5.17
PFO model	**R^2**	**K constant**		
	0.9928	-0.019		

Thermodynamic Investigations

Adsorption thermodynamics includes two types of parameters. Firstly, those which can be measured directly through experiments such as temperature and constants. Secondly, those which are measured indirectly through experimental data from slopes and intercepts of plots. These include free energy change (ΔG), enthalpy change (ΔH), entropy change (ΔS) and energy of the system. Studying these parameters is important to evaluate feasibility and validity of adsorption process for desired separation.

Gibbs free energy change is given in the equation as follows:

$$\Delta G = -RT\ln k \quad (13)$$

ΔG; free energy change described in J/mol, R; universal constant (8.314 J/mol) T; temperature in K. Its equation with ΔH and ΔS is as under:

$$\Delta G = \Delta H - T\,\Delta S \quad (14)$$

By combining the above equations (eq. 13 and eq. 14) we get:

$$\ln k = \Delta S/R - \Delta H/RT \quad (15)$$

Where equilibrium constant 'k' is calculated as:

$$k = Cad/\,Ce \quad (16)$$

A plot among log Cad/Ce v 1/T provide values of ΔH & ΔS from slope and intercept respectively. Gibbs free energy (ΔG) was calculated from experimental data at varying temperature range.

These parameters have either negative values or positive values depending upon experimental data.

When ΔH value is positive, adsorption process is endothermic, and negative value of ΔH suggests exothermic process. Physical and chemical sorption are also described by ΔH values. Adsorption process is physical in nature, when heat of adsorption is lesser than 80 kj/mol (similar to values of condensation energy), this is called as physio sorption. While, values higher than 80 kJ/mol correspond to chemisorption.

Positive value of ΔS refer to an increase in adsorption process, due to more uptake of adsorbate ions onto adsorbent surface. It also assumes some change in structural form of adsorbate and adsorbent during interaction, due to random motion of adsorbate species and increased interaction with adsorbent. Negative value of ΔS suggest a decrease in adsorption of adsorbate species on adsorbent surface, due to decrease in random motion of adsorbate species and less interaction among adsorbent and adsorbate.

Gibbs free energy ΔG values exhibits, spontaneity of an adsorption process upon change in temperature. Negative values of ΔG correspond to feasible adsorption and a spontaneous process, whereas, positive value of ΔG indicates non-spontaneous process and difficult adsorption.

Thermodynamic Study for Adsorption of Cr(Iii) onto:

SM, SMBC and HLSMBC

Experimental measurements were reviewed to determine thermodynamic parameters for adsorption of chromium metal onto SM, SMBC and HLSMBC. Gibbs free energy, entropy and enthalpy data serves as a benchmark in describing adsorption thermodynamics and heat of adsorption. Gibbs free energy trend is shown in Table. 10. for all the adsorbents, indicating

decrease in negative values is greater for SMBC>HLSMBC>SM. Enthalpy and entropy values are also given in Table. 10 to reveal nature of sorption process as either endothermic or exothermic and ease of process to displace water molecules by metal ions to adsorb on adsorbent surface. These values are in the order SM<HLSMBC<SMBC, with high values of SMBC for chromium removal.

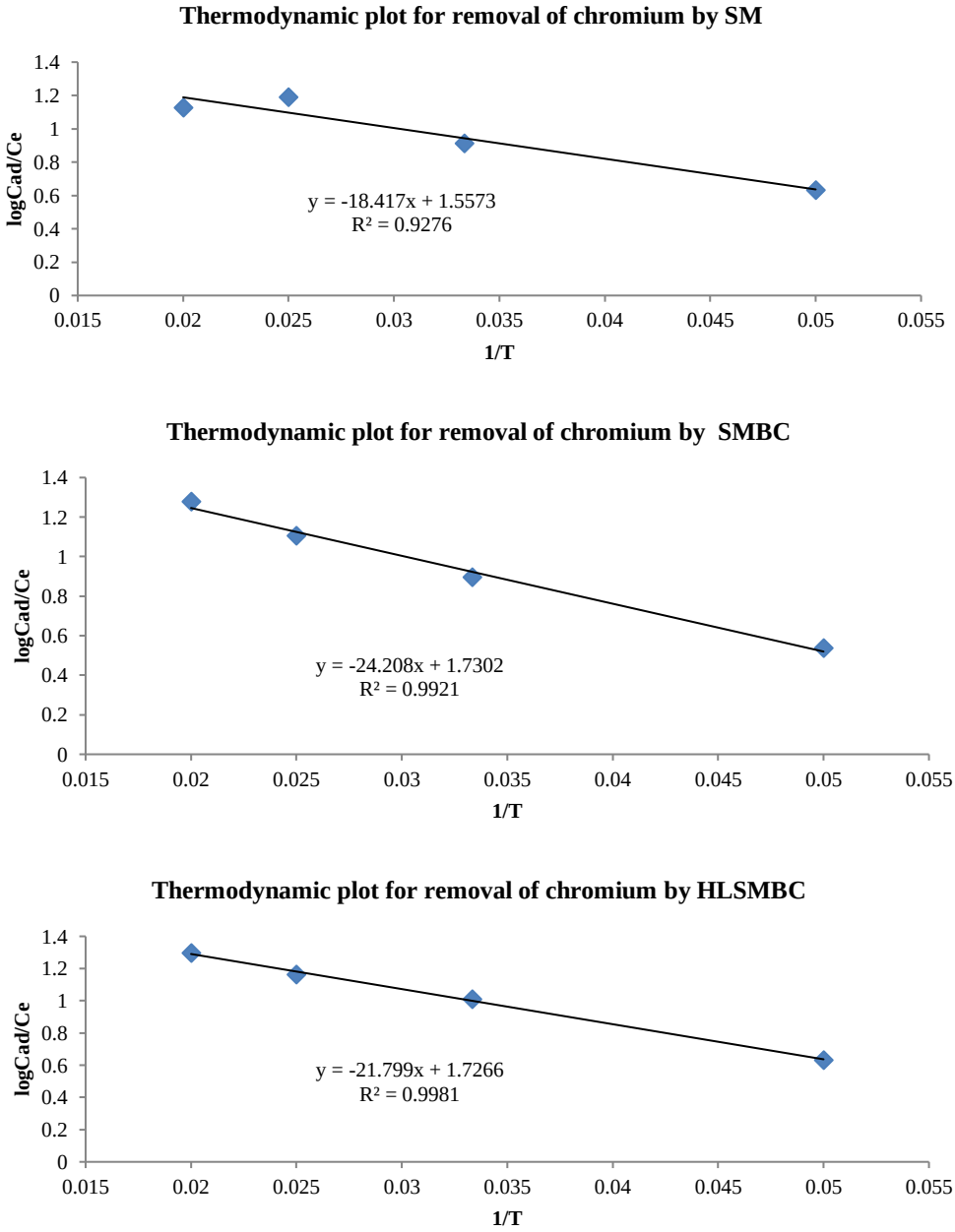

Fig. 15. Thermodynamic study for adsorption of Cr(III) onto: a. SM; b. SMBC; c. HLSMBC

Table 10. Thermodynamic parameters for adsorption of chromium on SM, SMBC & HLSMBC. *Thermodynamic calculations for chromium removal*

Adsorbents	Enthalpy change (ΔH)	Entropy change (ΔS)	Free energy change ΔG	Temperature (K)
			-472.57	293
Saccharum munja	18.42	1.55	-488.07	303
			-503.57	313
			-526.82	328
			-531.09	293
Saccharum munja BC	24.20	1.73	-548.39	303
			-565.69	313
			-591.64	328
			-525.75	293
HL Saccharum munja BC	21.79	1.72	-542.95	303
			-560.15	313
			-585.95	328

Desorption Study

In Desorption study adsorbent was recovered to be used again for experiments. This study also recover metal from adsorbent and that metal could be used again.

Table 11. Determination of % desorption of cr(III) from aqueous filtrate

	first	second	third	fourth	fifth
Saccharum munja	89.0	85.0	82.0	77.0	74.0
Saccharum munja BC	90.0	85.4	83.2	75.0	72.0
HL Saccharum munja BC	95.0	92.0	88.0	85.0	81.0

For chromium desorption after first wash removal percentage was observed to be 89%, 90%,95% for SM, SMBC and HLSMBC respectively.

Conclusion

In this work hematite loaded *Saccharum munja* was found as an efficient sorbent material for adsorption of chromium metal. Batch wise adsorption study was carried out for equilibrium isotherms, error function analysis, kinetic and thermodynamic investigations. Of these experimental and calculated results Freundlich model supported the best fit to adsorption data with high value of coefficient of determination. Error studies were calculated for five errors i.e. Sum Square of errors (ERRSQ), Average relative error (ARE), absolute error (EABS), chi-square test (X^2), Average percentage error (APE). Of these all errors revealed low values for all sorbents indicating favorable experimental results for removal of chromium metal. Of all chi-square test provided minimum error value results. Kinetic and thermodynamic studies revealed adsorption process with changing time and temperature parameters.

Acknowledgment

Department of chemistry, University of Sargodha, Sargodha, Pakistan, provided all support regarding use of chemicals and instruments for development of research work.

References

[1] J. Lehmann, S. Joseph, *Biochar for Environmental Management, Earth scan*, London, Sterling VA, 2009.

[2] J. Laine, S. Simoni, R. Calles, *Preparation of activated carbon from coconut shell in a small scale cocurrent flow rotary kiln*, **Chemical Engineering Communication**, 1991, 99, pp. 15-23.

[3] J. Wildman, F. Derbyshire, *Origins and functions of macroporosity in activated carbons from coal and wood precursors*, **Fuel**, 1991, 70, pp. 655-661.
[4] B. E. Warren, *X-ray diffraction in random layer lattices*, **Physical Review**, 1941, 59, pp. 693.
[5] R. Qadeer, J. Hanif, M. Saleem, M. Afzal, *Characterization of activated-charcoal*, **Journal of Chemical Society of Pakistan,** 1994, 16, pp. 229-235.
[6] R.C. Bansal, J.B. Donnet, F. Stoeckli, *Active carbon*, Marcel Dekker, New York, 1988.
[7] C.J. Atkinson, J.D. Fitzgerald, N.A. Hipps, *Potential mechanisms for achieving agricultural benefits from biochar application to temperate soils: a review*, **Plant Soil**, 2010, 337, pp.1-18.
[8] X. Guo, A. Liu, J. Lu, X. Niu, M. Jiang, Y. Ma, X. Liu, M. Li, *Adsorption mechanism of hexavalent chromium on biochar: kinetic, thermodynamic, and characterization studies*, **ACS omega**, 2020, 5(42), pp. 27323-27331.
[9] H. Sadegh, G.A. Ali, V.K. Gupta, A.S.H. Makhlouf, R. Shahryari-Ghoshekandi, M.N. Nadagouda, M. Sillanpaa, E. Megiel, *The role of nanomaterials as effective adsorbents and their applications in wastewater treatment*, **Journal of Nanostructure in Chemistry**, 2017, 7(1), pp. 1-14.
[10] L.R. Marcelo, J.S. de Gois, A.A. da Silva, D.V. Cesar, *Synthesis of iron-based magnetic nanocomposites and applications in adsorption processes for water treatment: a review*. **Environmental Chemistry Letters**, 2021, 19(2), pp. 1229-1274.
[11] R. Janani, B. Gurunathan, K. Sivakumar, S. Varjani, H.H. Ngo, E. Gnansounou, *Advancements in heavy metals removal from effluents employing nano-adsorbents: way towards cleaner production*, **Environmental Research**, 2022, 203, pp. 111815.
[12] S. Kajitani, H.L. Tay, S. Zhang, C.Z. Li, *Mechanisms and kinetic modelling of steam*, 2013.
[13] E.I. Ugwu, O. Tursunov, D. Kodirov, L.M. Shaker, A.A. Al-Amiery, I. Yangibaeva, F. Shavkarov, *Adsorption mechanisms for heavy metal removal using low cost adsorbents: A review*, **Earth and Environmental Science**, 2020, 614, pp. 012166.
[14] A.U. Rehman, S. Nazir, R. Irshad, K. Tahir, K. ur Rehman, R.U. Islam, Z. Wahab, *Toxicity of heavy metals in plants and animals and their uptake by magnetic iron oxide nanoparticles*, **Journal of Molecular Liquids,** 2021, 321, pp.114455.
[15] Y. Chen, K. Fu, S. Zhu, W. Luo, Y. Wang, Y. Li, E. Hitz, Y. Yao, J. Dai, J. Wan, V.A. Danner, T. Li, L. Hu, *Reduced graphene oxide films with ultrahigh conductivity as Li-ion battery current collectors*, **Nano Letters**, 2016, 16, pp. 3616-3623.
[16] M. Lippman, *Book on Asbestos and Mineral Fibres*, Elsevier Publishers, 1991, pp. 34-134.
[17] C. Liosis, A. Papadopoulou, E. Karvelas, T.E. Karakasidis, I.E. Sarris, *Heavy Metal Adsorption Using Magnetic Nanoparticles for Water Purification: A Critical Review*. **Materials**, 2021, 14(24), pp. 7500.
[18] M. Muchuweti, J.W. Birkett, E. Chinyanga, R. Zvauya, M.D. Scrimshaw, *J.N. Lester, Heavy metal content of vegetables irrigated with mixtures of wastewater and sewage sludge in Zimbabwe: implications for human health*, **Agriculture, Ecosystem and Environment**, 2006, 112, pp. 41-48.
[19] Michalak, K. Chojnacka, A. Witek-Krowiak, *State of the art for the biosorption process—a review*, **Applied Biochemistry and Biotechnology**, 2013, 170, pp. 1389-1416.
[20] K. Liu, Z. Nie, N. Zhao, W. Li, M. Rubinstein, E. Kumacheva, *Step-growth polymerization of inorganic nanoparticles*, **Science,** 2010, 329, pp. 197-200.
[21] R. Bushra, A. Ahmed, M. Shahadat, *Mechanism of adsorption on nanomaterials*, **Advanced Environmental Analysis**, 2016, pp. 90-111.
[22] V.K. Gupta, A. Rastogi, A. Nayak, *Adsorption studies on the removal of hexavalent chromium from aqueous solution using a low cost fertilizer industry waste material*, **Journal of Colloid and Interface Science**, 2010, 342, pp. 135-14.
[23] Q.L. Feng, J. Wu, G.Q. Chen, F.Z. Cui, T.N. Kim, J.O. Kim, *A mechanistic study of the antibacterial effect of silver ions on Escherichia coli and Staphylococcus aureus*, **Journal of Biomedical Materials Research**, 2000, 52, pp. 662-668.

[24] T. Iqbal, S. Iqbal, F. Batool, D. Thomas, M.H. Iqbal, *Utilization of a newly developed nanomaterial based on loading of biochar with hematite for the removal of cadmium ions from aqueous media*, **Sustanability**, 2021, 13(4), pp. 2191.
[25] L. T. Popoola, L.T. *Characterization and adsorptive behaviour of snail shell-rice husk (SS-RH) calcined particles (CPs) towards cationic dye*. **Heliyon**., 2019**, 5, e01153**.
[26] T.M. Elmorsi, *Equilibrium isotherms and kinetic studies of removal of methylene blue dye by adsorption onto miswak leaves as a natural adsorbent*, **Journal of Environmental Protection**, 2011, 2, pp. 817-827.
[27] E. Richter, S. Wilfried, A.L. Myers, *Effect of adsorption equation on prediction of multicomponent adsorption equilibria by the ideal adsorbed solution theory*, **Chemical Engineering Science**, 1989, 44, pp. 1609-1616.
[28] Günay, E. Arslankaya, I. Tosun, *Lead removal from aqueous solution by natural and pretreated clinoptilolite: adsorption equilibrium and kinetics*, **Journal of Hazardous Material**, 2007, 146, pp. 362-371.
[29] Theivarasu, S. Mylsamy, *Removal of malachite green from aqueous solution by activated carbon developed from cocoa (Theobroma Cacao) shell-A kinetic and equilibrium studies*, **Journal of Chemistry**, 2011, 8, pp. S363-S371.
[30] M. Gubernak, W. Zapala, K. Kaczmarski, *Analysis of amylbenzene adsorption equilibria on an RP-18e chromatographic column*, **Acta Chromatograph**, 2003, 13, pp. 38-59.
[31] D.N. Leonard, G.W. Chander, S. Seraphin, *Scanning Electron Microscopy*, 2012.
[32] K. Torres-Rivero, J. Bastos-Arrieta, N. Fiol, A. Florido, *Metal and metal oxide nanoparticles: An integrated perspective of the green synthesis methods by natural products and waste valorization: applications and challenges*, **Comprehensive Analytical Chemistry**, 2021, 94, pp. 433-469.
[33] P.M. Shameer, P.M. Nishath, *Exploration and enhancement on fuel stability of biodiesel: A step forward in the track of global commercialization*, **Advanced Biofuels**, 2019, pp. 181-213.
[34] O.P. Choudhury, Priyanka, *Scanning Electron Microscope: Advantages and Disadvantages in Imaging Components*, **International Journal of Current Microbiology and Applied Sciences**, 2017, 6, pp.1877-1882.
[35] Oros, J. Krstić, I. Kovačević, *Adsorption feasibility in the Cr (total) ions removal from waste printing developer*, **Global Nest Journal**., 2012, 14, pp. 18-23.

Received: January 13, 2022
Accepted: February 21, 2022